J. Fluid Mech. (2025), *vol.* 1016, R4, doi:10.1017/jfm.2025.10293

Predicting internal boundary layer growth following a roughness change in thermally neutral and stable boundary layers

Shan-Shan Ding[1,2], **Matteo Carpentieri**[1], **Alan Robins**[1] and **Marco Placidi**[1]

[1]EnFlo laboratory, School of Mechanical Engineering Sciences, University of Surrey, Guildford GU2 7XH, UK

[2]Atmospheric Oceanic and Planetary Physics, Department of Physics, University of Oxford, Oxford OX1 3PU, UK

Corresponding authors: Shan-Shan Ding, shanshan.ding@physics.ox.ac.uk; Marco Placidi, m.placidi@surrey.ac.uk

(Received 2 March 2025; revised 8 April 2025; accepted 25 April 2025)

This study uses the diffusion analogy (Miyake, *Sci. Rep.*, 5R-6, 1965, Univ. of Washington, Seattle, USA) to predict the full growth behaviour of internal boundary layers (IBLs) induced by a roughness change for neutrally – and especially stably – stratified boundary layers with finite thickness. The physics of the diffusion analogy shows that the streamwise variation of the IBL thickness is dictated by σ_w/U at the interface, where σ_w and U represent wall-normal Reynolds stress and mean streamwise velocity, respectively. The existing variants of the model, summarised by Savelyev & Taylor (2005, *Boundary-Layer Meteorol.,* vol. 115, pp. 1–25), are tailored to IBLs confined within the constant shear stress layer. To extend the applicability of the model to the outer region, we investigate the relation between σ_w/U and U/U_∞ in the outer region across varying stratification, where U_∞ is the free-stream velocity. Our analysis reveals that wind tunnel data from a number of facilities collapse onto a master curve when σ_w/U is premultiplied by a height-independent parameter, which is a function of the ratio of Monin–Obukhov length to the boundary layer thickness. The scaled σ_w/U decreases inversely with U/U_∞ in the surface layer, transitioning to a linear decrease as U/U_∞ increases. The new model, which integrates these findings, along with the effects of streamline displacement and acceleration, captures the complete characteristics of IBLs as they develop within turbulent boundary layers of finite thickness.

Key words: turbulent boundary layers, stratified flows, atmospheric flows

1. Introduction

Changes in the aerodynamic or thermal properties of surfaces beneath the atmospheric boundary layer generate an interface capping an internal boundary layer (IBL), where the energy and momentum fluxes reflect a blend of characteristics from the surfaces before and after the change. Examples of the transition include flows from rural to urban regions, from sea to land, and from sea to ice cap (and vice versa), which influence the local pollutant dispersion and meteorology (Baklanov *et al.* 2011). Studying the IBL is beneficial for applications such as weather prediction, pollutant management and wind energy optimisation. Consequently, the accurate prediction of the IBL growth curve has been a longstanding research focus (Garratt 1990; Bou-Zeid *et al.* 2020), especially when the boundary layer is coupled with multiple physical processes and on different length scales.

A paradigm model for studying kinetic IBLs emphasises an abrupt change in surface roughness along the streamwise direction, where the surface downstream of the change has the roughness length z_{02}, and upstream of the change z_{01}. Predicting the development of the adjusted layer, i.e. the variation of its thickness δ_i along the streamwise fetch x, begins with an important simplification, namely that this layer is embedded within the constant shear stress region.

Miyake (1965) proposed a passive diffusion analogy, which links the IBL growth to the vertical dispersion of a passive plume. The IBL's growth rate $\mathrm{d}\delta_i/\mathrm{d}t$ is prescribed by σ_w, i.e. the standard deviation of the wall-normal velocity w at the interface. Using the chain derivative rule $\mathrm{d}x = U\,\mathrm{d}t$ leads to $U(\mathrm{d}\delta_i/\mathrm{d}x) = A\sigma_w$, where σ_w is a height-independent value as the IBL lies within the constant shear stress layer. The constant A is model-dependent, though Savelyev & Taylor (2001) revealed that it increases with $M \equiv \ln(z_{02}/z_{01})$ by studying a large number of datasets. The relationship between A and M is associated with the effect of streamlines displacement across the step change in roughness, which was accounted for by incorporating the mean wall-normal velocity into the model by Savelyev & Taylor (2005). In the same work, they extended the model to diabatic conditions by integrating the Monin–Obukhov similarity (MOST) (Monin & Obukhov 1954) to predict the development of the IBL across a change in the Monin–Obukhov length.

The simplified scenario considered in the aforementioned model becomes less effective when the outer edge of the IBL exceeds the surface layer height due to the deviation of the mean streamwise velocity from the logarithmic law (MOST) for neutral (stable) flows, and the significant variation of σ_w with height. Conventionally, the height–fetch ratio estimated by these small fetch models was employed to predict the complete evolution of the IBL (i.e. through the whole boundary layer) assuming the absence of Coriolis force effects (Garratt 1990). However, in wind tunnel studies, the overprediction of the IBL formulae from the physical models was remarkable, with surface changes from rough to smooth (Li *et al.* 2022) and rough to rougher in neutral conditions (Gul & Ganapathisubramani 2022) and in stable conditions (Ding *et al.* 2023). For neutral stratification, Li *et al.* (2022) predicted a shallower IBL in the outer region by developing the physical model initially proposed by Elliott (1958) for the logarithmic layer in the context of a finite-thickness boundary layer. They consider the modification of streamwise momentum within the IBL to be dictated by the decrease in the shear stress across this region. Accounting for the decay of the shear stress with height, the wake function, and the thickening process of the boundary layer collectively slow the IBL growth in the outer region.

However, to the authors' knowledge, there is no existing physical model that captures the complete growth of the IBL (irrespective of the relative depth of the IBL compared

Case	Re	Ri_b	z_{01}/δ	L_{01}/δ	z_{02}/δ	L_{02}/δ
N1	4.5×10^4	–	1.9×10^{-4}	∞	2.3×10^{-3}	∞
N2	3.0×10^4	–	3.9×10^{-4}	∞	7.1×10^{-3}	∞
S1	4.5×10^4	0.13	1.2×10^{-4}	1	1.2×10^{-3}	1.9
S2	3.0×10^4	0.27	1.3×10^{-4}	0.6	2.9×10^{-3}	1.2

Table 1. Dimensionless parameters for the cases studied: Re, Ri_b, z_{01}/δ and L_{01}/δ are for the incoming flow, while z_{02}/δ and L_{02}/δ for the downstream flow.

to the surface layer) for stable thermal stratification. Whether or not the diffusion analogy can accurately capture the characteristics of the IBL in the outer region, especially under stable conditions, has yet to be decided. To address this question, we investigate the impact of stable stratification on σ_w/U and U within the boundary layer using data measured in different wind tunnels. Subsequently, we develop a modified diffusion model that can accommodate any IBL depth.

2. Cases studied

We focus on surface roughness changes from rough (z_{01}) to rougher ($z_{02} > z_{01}$) using the published data in Ding *et al.* (2024, 2024). Only the essential information relevant to this paper is included below; additional details can be found in the referenced papers. Streamwise velocity ($\tilde{u} = U + u$) and vertical velocity ($\tilde{w} = W + w$) were measured using laser Doppler anemometry. Here, (U, W) denotes the mean value, and (u, w) denotes the fluctuations. Profiles along the wall-normal direction z were measured in the central plane of the wind tunnel, where the origin of the coordinates is set at the roughness change on the floor. The aerodynamic parameters of the incoming flow were measured at 0.76 m upstream of the step change in roughness.

Four cases, comprising two neutrally and two stably stratified boundary layers, were investigated. The characteristics of the incoming flows and the roughness length change are summarised in table 1. In the table, the Reynolds number is $Re = U_\infty \delta/\nu$, where ν denotes the kinematic viscosity, U_∞ denotes the free-stream velocity, and δ denotes the boundary layer thickness determined by the mean streamwise velocity reaching 99 % of the free-stream velocity U_∞. The bulk Richardson number is $Ri_b = (g(\Theta_\delta - \Theta_0)\delta)/\Theta_0 U_\delta^2$, where Θ_0 denotes the absolute surface temperature, g is gravitational acceleration, and Θ_δ (U_δ) denotes the mean temperature (streamwise velocity) at the top of the boundary layer. The surface Monin–Obukhov length is $L_0 = u_*^2 \Theta_0/(g\kappa\theta_*)$ and is a measure of the height at which stability leads to significant reductions in vertical turbulence. Here, u_* (θ_*) represents the friction velocity (temperature).

For both neutral and stable cases, the IBL depth was determined from the merging point of the local wall-normal profile of $\sigma_u^2(z)$ with its counterpart upstream of the roughness change. This methodology is consistent with identifying the 'knee' point in the mean streamwise velocity profile (Li *et al.* 2022; Ding *et al.* 2023). Here, σ_u denotes the standard deviation of the streamwise velocity. This methodology, and the subsequent analysis in § 3, relies on the assumption of spanwise homogeneity, which was demonstrated in the region above the roughness sublayer (Ding *et al.* 2024).

Variation in the degree of stratification, conventionally induced by the change in wall temperature or heat flux, can generate a thermal IBL that caps a region with modified mean temperature or heat flux (Garratt 1990). The cases discussed here do not present any discontinuity in the surface thermal condition; across the roughness, change L_0/δ varies from 1.0 to 1.9 for case S1, and from 0.6 to 1.2 for case S2. This variation in the stratification is not significant as the thermal IBL passively follows the kinetic IBL (Ding *et al.* 2024). Thus we focus on the latter in the following analysis.

3. Results and discussion

3.1. *Predicting wall-normal turbulent intensity profiles in stable flows*

To extend the diffusion analogy to the outer region, we begin with analysis of σ_w/U. Figure 1(*a*) shows σ_w/U as a function of U/U_∞ (the lower branch) for the logarithmic regions and beyond, which are the target predictive regions. The curves of σ_w/U in stable cases were scaled by a height-independent parameter σ_L to collapse results onto the neutral ones. The value of σ_L was determined by minimising the difference between $\sigma_L\sigma_w/U$ for the stable case and σ_w/U for neutral cases in the region of interest. The parameter, σ_L, measures the suppression of the wall-normal component of normal stress due to stable stratification. As shown in figure 1(*c*), σ_L decreases monotonically as L_0/δ increases. Moreover, data from different datasets fall onto a unique function in the form $\sigma_L = 0.9256e^{-L_0/\delta} + 1$. This exponential decay is demonstrated by the linear function in the semi-log plot in figure 1(*d*). However, the relation between σ_L and Ri_b is sensitive to the system investigated, as shown in figure 1(*b*).

Figure 1(*a*) demonstrates good data collapse as $\sigma_L\sigma_w/U$ varies with U/U_∞ consistently in all cases. In the logarithmic layer, the attached-eddy hypothesis proposed by Townsend (1976, pp. 144–145) prescribes that σ_w is independent of z. This height invariance is a foundational assumption in the diffusion analogue model, where σ_w is typically taken as $1.25u_*$ within the region extending from $z = z_{02}$ (where $U/U_\infty \sim 0.1M$) to the upper bound of the logarithmic layer. This assumption leads to $\sigma_w/U \sim U^{-1}$. Preserving this relationship within (3.1) below ensures that the model in § 3.3 approaches the classical one as $U \to 0$ for an infinitely small M, since all terms of order $\sim o(U^n)$ (with $n \geqslant 1$) vanish in the aforementioned limit. In the wake region ($0.75 \leqslant U/U_\infty$), $\sigma_L\sigma_w/U$ decreases approximately as a linear function of U/U_∞. These trends are consistent with previous observations of boundary layers on smooth surfaces under neutral (Flack, Schultz & Shapiro 2005) and stable (Williams *et al.* 2017) conditions. To delineate the complete trend, we propose a composite function

$$\frac{\sigma_L\sigma_w}{U} = a_0\left(\frac{U}{U_\infty}\right)^{-1} - a_1\frac{U}{U_\infty}, \tag{3.1}$$

where $a_0 = 0.0693$ and $a_1 = 0.0476$ are fitting parameters for the master curve shown in figure 1(*a*). We expect this curve to be valid for different rough walls provided that they obey Townsend's similarity hypothesis (Flack *et al.* 2005, 2007).

Figure 1(*a*) also demonstrates $\sigma_L\sigma_u/U$ as a function of U/U_∞. Here, the collapse onto a master linear curve is poorer than seen for the wall-normal components. Their relation within $0.7 < U/U_\infty < 1$ follows the empirical function, i.e. $\sigma_u/U = 0.286 - 0.255U/U_\infty$, identified by Alfredsson, Segalini & Örlü (2011) for neutral boundary layers over smooth surfaces. The curve becomes steeper with increasing roughness (Castro 2013). This observation suggests that the empirical function could be reliably employed to $\sigma_L\sigma_u/U$ in stable boundary layers over smooth or transitionally rough surfaces.

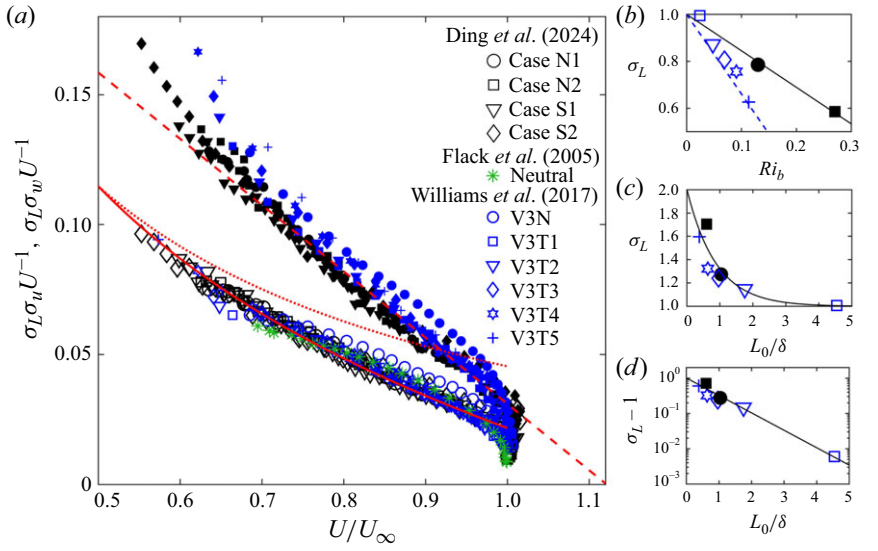

Figure 1. (*a*) Plots of $\sigma_L\sigma_w U^{-1}$ (lower branch, empty symbols) and $\sigma_L\sigma_u U^{-1}$ (upper branch, solid symbols) as functions of U/U_∞. The red dotted line indicates $(U/U_\infty)^{-1}$. The red solid curve is the fit by (3.1). The red dashed line is the relation proposed by Alfredsson *et al.* (2011). Plots of σ_L as a function of (*b*) bulk Richardson number Ri_b and (*c*) L_0/δ. (*d*) Plot of $\sigma_L - 1$ as a function of L_0/δ. In (*b,c,d*), solid circles (squares) are for case S1 (S2) from Ding *et al.* (2024), and empty symbols are from Williams *et al.* (2017) with the notation in (*a*).

3.2. *Empirically modelling mean profiles of streamwise velocity*

Figure 2(*a*) demonstrates that the effect of stratification on the mean streamwise velocity profiles is restricted within $z_c/\delta < 0.25$ as U/U_∞ therein is sensitive to the degree of stratification. We define z_c as a precise measure of the thickness of the layer where the mean streamwise velocity is significantly influenced by stratification. In the region beyond z_c, U/U_∞ is barely altered by the stratification (variations within 4 %), as shown in figure 2(*a*). This suggests that the wake function in adiabatic conditions can be used extensively for stably stratified boundary layers. Therefore, we employ MOST in the region $z < z_c$ (under the assumption that the thickness of the surface layer with a constant flux equals z_c), thus the stability function ϕ_m, which links the gradient of mean streamwise velocity to the surface momentum flux in the form $\phi_m = (\kappa z/u_*)(\mathrm{d}U/\mathrm{d}z)$, was modified to $\phi_m(z/L_0) = 1 + (\beta_m z/(2L_0))\,\mathrm{erfc}((z - z_c)/s)$. Integrating $\mathrm{d}U/\mathrm{d}z$ from z_0 and adopting the wake function (Jones, Marusic & Perry 2001) constructs the complete vertical profile of U/U_∞ assuming a negligible zero-plane displacement (this assumption restricts the applicability of this approach in large urban settings, where the zero-plane displacement can be significant, but it is reasonable in many atmospheric flows):

$$U_n \equiv \frac{U}{U_\infty} = \sqrt{\frac{C_f}{2}}\frac{1}{\kappa}\left\{\ln\frac{z}{z_{01}} + \frac{\beta_m}{L_0}\Phi(z, z_c, s) + \Pi\left[2\left(\frac{z}{\delta_c}\right)^2\left(3 - \frac{2z}{\delta_c}\right)\right] - \frac{1}{3}\left(\frac{z}{\delta_c}\right)^2\right\}, \tag{3.2}$$

where $\Phi = \int_{z_{01}}^{z}(1/2)\,\mathrm{erfc}((l - z_c)/s)\,\mathrm{d}l$. The skin-friction coefficient is $C_f = 2\rho_w u_*^2/(\rho_\infty U_\infty^2)$, with ρ_w (ρ_∞) the air density at the wall (in the free stream). Here, $\beta_m = 8$ for the studied flows (Hancock & Hayden 2018), Π represents the wake factor, and s measures the width of the transition region between two layers with or without significant

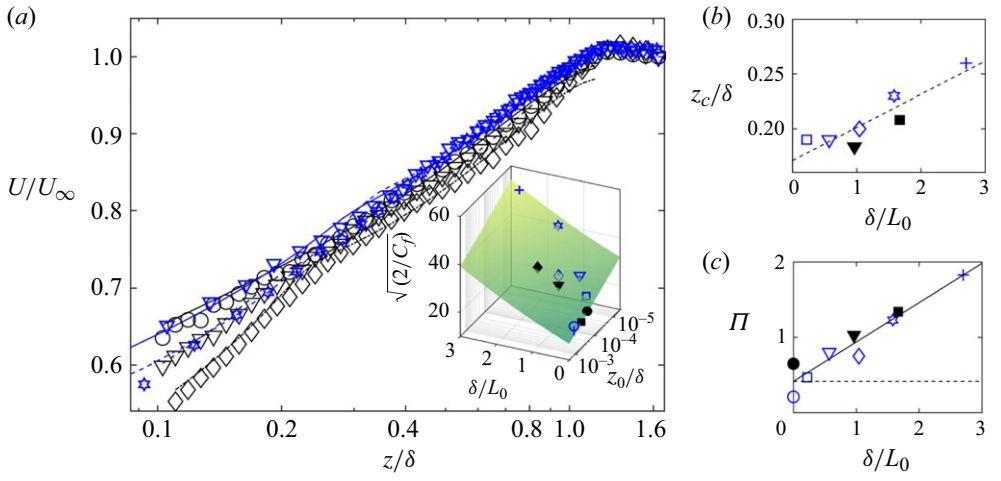

Figure 2. (*a*) Wall-normal profiles of the mean streamwise velocity under varying stable stratification. Solid (dash-dotted) curves are fits of (3.2). The inset shows $\sqrt{C_f/2}$ as a function of z_0/δ and δ/L_0. The vertical bar on each symbol represents the difference between the measured value and the prediction from (3.4) (coloured surface). (*b*) The upper edge of the region under the effect of MOST z_c/δ. (*c*) The wake strength Π as a function of δ/L_0. Symbols as in figure 1.

influences of stratification, being approximately $0.1z_c$ for stable cases. The real boundary layer thickness δ_c approximates 1.2δ for cases studied. Figure 2(*a*) shows a range of measured data against (3.2).

Marusic *et al.* (2015) found that Π is independent of the streamwise location for fully developed neutral boundary layers. Herein we use the terminology 'fully developed' to refer to boundary layers that are fully adjusted to the underlying surface and whose characteristics are slowly varying in the streamwise direction. Hancock & Hayden (2018) noted the invariance of wall-normal profiles of mean streamwise velocity with streamwise locations for fully developed stable boundary layers. Thus $U(z)/U_\infty$ should be dictated by $(\Pi, z_0/\delta, C_f, L_0/\delta, z_c/\delta)$. Substituting $z=\delta$ into (3.2) gives the relation between C_f and $(\kappa, \beta_m, z_0/\delta, L_0/\delta, \Pi, z_c/\delta)$:

$$\sqrt{\frac{2}{C_f}} = \frac{1}{\kappa}\left\{\ln\frac{\delta}{z_0} + \frac{\beta_m z_c/\delta}{L_0/\delta} + \Pi\left[2\left(\frac{1}{1.2}\right)^2\left(3-\frac{2}{1.2}\right)\right] - \frac{1}{3}\left(\frac{1}{1.2}\right)^2\right\}, \tag{3.3}$$

where $\Phi(\delta, z_c, s) = z_c$. Taking $\beta_m = 8$ and $\kappa = 0.41$, figure 2(*c*) shows that Π increases approximately as a linear function of δ_0/L_0, and thus is delineated by $\Pi = B_1 + B_2\delta/L_0$, with $B_1 \approx 0.485$ and $B_2 \approx 0.51$. In neutral conditions, Π approaches 0.485 (0.42 for $\kappa = 0.384$). Substituting the above relation and $z_c/\delta = 0.185 + 0.027\delta/L_0$ (figure 2*b*) into (3.2) leads to a simplified relationship of C_f with z_0/δ and L_0/δ for the cases studied:

$$\sqrt{\frac{2}{C_f}} = \frac{1}{0.41}\left[-\ln\left(\frac{z_0}{\delta}\right) + 0.22\frac{\delta^2}{L_0^2} + 2.42\frac{\delta}{L_0} + 0.67\right]. \tag{3.4}$$

Therefore, a complete velocity profile of a stably stratified boundary layer is determined by (3.2) and (3.4), given $(z_0/\delta, L_0/\delta)$ or $(C_f, L_0/\delta)$.

3.3. *A modified diffusion analogy*

The abrupt roughness change at the surface of a fully developed flow brings at least three distinct effects: (i) streamline displacement, (ii) acceleration/deceleration of flow influencing the mean velocity field (Townsend 1976), and (iii) a local breakdown of the turbulence dynamics leading to an imbalance of turbulence production and dissipation. All three processes can be modulated by the strength of the roughness discontinuity, M. Antonia & Luxton (1971) noted that the roughness change can induce a large vertical gradient of mean streamwise velocity and turbulent intensity, leading to enhanced turbulence production and turbulent diffusion that are predominantly balanced by the advection of turbulent energy. Savelyev & Taylor (2005) incorporated the mean wall-normal velocity into the diffusion analogy by accounting for the streamline displacement, which was formulated as

$$U\,\frac{\mathrm{d}\delta_i}{\mathrm{d}x} = C_1\sigma_w + C_2 W. \tag{3.5}$$

We now briefly review the process to derive the IBL formulae in Savelyev & Taylor (2005) in the circumstance of the roughness length, friction velocity and Monin–Obukhov length changing from (z_{01}, u_{*1}, L_{01}) to (z_{02}, u_{*2}, L_{02}). The mean vertical velocity W is approximated as $-\Delta U\delta_i/x$ using the continuity constraint, where ΔU represents the difference between the local mean streamwise velocity at $z=\delta_i$ and the corresponding value before the roughness change. The expression for ΔU at δ_i reads $(u_{*2}/\kappa)(\ln(\delta_i/z_{02}) + \beta_m(\delta_i - z_{02})/L_{02}) - (u_{*1}/\kappa)(\ln(\delta_i/z_{01}) + \beta_m(\delta_i - z_{01})/L_{01})$ for neutrally and stably stratified boundary layers. Replacing u_{*2} with u_{*1} simplifies the expression for W_s (W induced by the streamwise displacement) to

$$W_s = \frac{\delta_i}{x}\frac{u_{*1}}{\kappa}\left[M + \beta_m\frac{\delta_i - z_{01}}{L_{01}} - \beta_m\frac{\delta_i - z_{02}}{L_{02}}\right]. \tag{3.6}$$

In the case of a neutral boundary layer, L_{01} and L_{02} approach infinity. Assuming $\sigma_w/u_{*1} = C_0$, which is reasonable in a constant shear stress layer, the right-hand side of (3.5) can be adjusted to $C_1\sigma_{w1}(1 + (C_2/C_1)(W_s/C_0u_{*1}))$, yielding (36) in Savelyev & Taylor (2005). This formula will hereafter be referred to as the ST model, where $C_1 = 1$, $C_2 = \kappa C_0 \approx 0.51$ ($C_0 \approx 1.25$).

To study the impact of the decay in wall-normal stress, we adopt (3.1) and substitute (3.6) into (3.5), giving

$$\frac{\mathrm{d}\delta_i}{\mathrm{d}x} = \frac{a_0{U_n}^{-1} - a_1U_n}{\sigma_L} + C_2\frac{\delta_i}{x}\left(M + \beta_m\frac{\delta_i - z_{01}}{L_{01}} - \beta_m\frac{\delta_i - z_{02}}{L_{02}}\right)\frac{\sqrt{C_f}}{\sqrt{2}\,\kappa U_n}. \tag{3.7}$$

This is solved by the fourth-order Runge–Kutta algorithm (ode45 in MATLAB), with the integration initiated at $x = z_{01}$. The initial height of the IBL satisfies $\delta_i(\ln(\delta_i/\sqrt{z_{01}z_{02}}) - 1) = 0.5z_{01}$ (Savelyev & Taylor 2005). Here, we make the assumption that z_{01}/δ, Π_1 and L_{01}/δ are invariant with streamwise location, in line with a fully developed flow. Figure 3(*a*) benchmarks (3.7) to the dataset, showing a significant improvement in accuracy compared to the ST model.

After validating the model for neutrally stratified boundary layers, we next employ the model (3.7) to study the impact of thermal stability on the IBL development. For cases S1 and S2, Ding *et al.* (2023) found that the slightly negative mean wall-normal velocity in the outer region (being two orders of magnitude smaller than the free streamwise velocity) could greatly suppress the development of the IBL. The negative wall-normal flow likely originates from the presence of the favourable pressure gradient (Jones *et al.* 2001). We begin from (3.5) but then consider the wall-normal velocity,

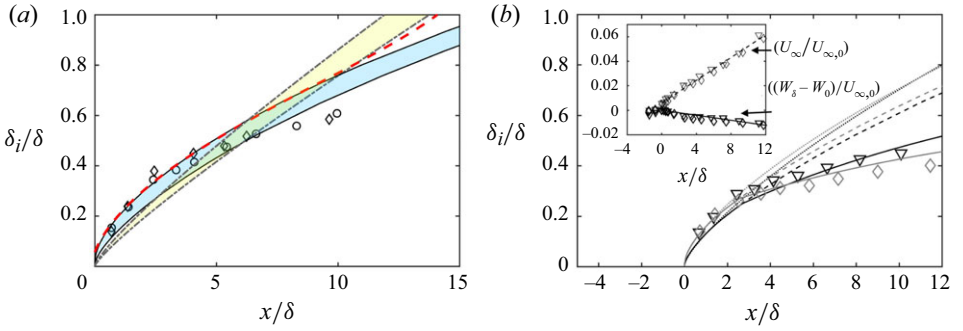

Figure 3. The IBLs for (*a*) neutrally stratified boundary layers and (*b*) stably stratified boundary layers. (*a*) Cases N1 and N2 with input parameters $(C_f, z_{01}/\delta, M)$ estimated for $\kappa = 0.41$. Symbols: circle, case N1; diamond, case N2. The bluish (yellowish) region with solid (dash-dotted) boundary curves represents the prediction from the ST model. The upper boundary curves in the coloured regions correspond to case N2, and the lower ones to case N1. The red dashed curve represents the prediction for case N1 from the finite-thickness boundary layer model (Li *et al.* 2022). (*b*) Cases S1 and S2. Dotted curves represent the prediction of the ST model; dashed curves indicate (3.7); solid curves indicate (3.10). The inset shows data on the upper branch representing $U_\infty/U_{\infty,0}$, and on the lower branch representing $(W_\delta - W_0)/U_{\infty,0}$; the dashed (solid) lines are linear fits. Symbols as in figure 1.

noting that this could also be induced by sources other than streamline displacement. To derive W, we rewrite the continuity equation in terms of dimensionless variables $\tilde{x} = x/\delta$ and $\tilde{z} = z/\delta$ using the chain derivative rules $\mathrm{d}U/\mathrm{d}x = (\mathrm{d}U/\mathrm{d}\tilde{x})(\mathrm{d}\tilde{x}/\mathrm{d}x) = (\mathrm{d}U/\mathrm{d}\tilde{x})((1/\delta) - (x/\delta^2)(\mathrm{d}\delta/\mathrm{d}x))$ and $\mathrm{d}W/\mathrm{d}z = (\mathrm{d}W/\mathrm{d}\tilde{z})(\mathrm{d}\tilde{z}/\mathrm{d}z) = (1/\delta)(\mathrm{d}W/\mathrm{d}\tilde{z})$. The integral of $\mathrm{d}W/\mathrm{d}\tilde{z} = -(\mathrm{d}U/\mathrm{d}\tilde{x})(1 - \tilde{x}(\mathrm{d}\delta/\mathrm{d}x))$ from the upper edge of the IBL to the top of the boundary layer, assuming that $U_n(z/\delta)$ therein remains invariant with streamwise locations, gives

$$W(x, \delta_i) = W(x, \delta) + \int_{\delta_i/\delta}^{1} \frac{\mathrm{d}U_\infty}{\mathrm{d}\tilde{x}} \left(1 - \frac{x}{\delta}\frac{\mathrm{d}\delta}{\mathrm{d}x}\right) U_n(l)\,\mathrm{d}l, \tag{3.8}$$

where $W(x, \delta)$ denotes the mean wall-normal velocity at the top of the boundary layer, $\mathrm{d}U_\infty/\mathrm{d}\tilde{x}$ is the effect of flow acceleration, and the second term in parentheses stands for the effect of the boundary layer thickening process. The inset of figure 3(*b*) shows that U_∞ and W at the upper edge of the boundary layer both vary with streamwise locations in an approximately linear way. Thus we adopt $W(x, \delta)/U_{\infty,0} = w_0 + w_1(x/\delta)$, and define a constant acceleration coefficient $K = \mathrm{d}(U_\infty/U_{\infty,0})/\mathrm{d}\tilde{x}$ for the cases studied. For both stable cases, (w_1, K) are $(-0.0010, 0.0055)$, and w_0 is -0.0073 for case S1, and -0.0133 for case S2. The flow acceleration observed herein is likely due to the combined effect of the increase in surface roughness and the boundary layer growth on all surfaces due to the fact that the facility does not have an adjustable roof to balance these effects. We note that vertical velocity and flow acceleration have typically been overlooked in previous studies, but a generalisation of the presented model to non-zero pressure gradient is foreseeable. Since the boundary thickening effect is an order of magnitude smaller than the acceleration effect, it can be neglected, simplifying (3.8) to

$$W_m(x, \delta_i) = U_{\infty,0}\left(w_0 + w_1\frac{x}{\delta} + K\int_{\delta_i/\delta}^{1} U_n(l)\,\mathrm{d}l\right). \tag{3.9}$$

In the above expression, W_m is estimated from the mean velocity measured at the edge of the boundary layer, and thus contains the effects of acceleration and streamline displacement due to roughness changes. Within the roughness sublayer, (3.9) can break

down due to three-dimensional roughness effects, while W_s is still effective for predicting the initial growth of the IBL (see ST model performance). Therefore, we replace W_s with (3.9) when the top edge of the IBL extends beyond $z_c + 3s$ (≈ 5.5 roughness element heights, in line with Schultz and Flack 2005). For these reasons, we suggest the following piecewise function:

$$\frac{\mathrm{d}\delta_i}{\mathrm{d}x} = \frac{a_0 U_n^{-1} - a_1 U_n}{\sigma_L} + \begin{cases} \dfrac{C_2}{U_n(\delta_i)} \dfrac{\sqrt{C_f}}{\sqrt{2}\,\kappa} \dfrac{\delta_i}{x} \left(M + \beta_m \dfrac{\delta_i - z_{01}}{L_{01}} - \beta_m \dfrac{\delta_i - z_{02}}{L_{02}} \right), \\ \qquad \delta_i \leqslant z_c + 3s, \\ \dfrac{C_2}{U_n(\delta_i)} \left[w_0 + w_1 \dfrac{x}{\delta} + K \displaystyle\int_{\delta_i/\delta}^{1} U_n(l)\,\mathrm{d}l \right], \\ \qquad \delta_i > z_c + 3s. \end{cases} \tag{3.10}$$

Figure 3(*b*) shows that (3.7) improves the accuracy of the prediction from the ST model, but overprediction still occurs; (3.10) instead well captures the shallow IBL in the outer region. Since the model has no free parameters, it could potentially predict neutrally or stably IBLs in the presence of flow acceleration induced by roughness change or other sources, given the mean velocity at the top of the boundary layer.

4. Conclusions

We have identified two features of stably stratified boundary layers over smooth and transitionally rough surfaces through the analysis of experimental data from a number of wind tunnel studies. First, the wall-normal profiles of outer-scaled mean streamwise velocity in the wake region remain nearly invariant regardless of the stratification, leading to an approximately linear increase in wake strength with increasing δ/L_0. Second, appropriately scaled profiles of wall-normal fluctuation ($\sigma_L \sigma_w / U$) as a function of U/U_∞ in the cases studied fall onto a unique curve, where the height-independent parameter $\sigma_L - 1$ decays exponentially with δ/L_0. By incorporating these two findings, and the effect of streamline displacement from Savelyev & Taylor (2005), we develop a new diffusion model applicable to the complete growth of the IBLs, irrespective of its depth in relation to the local boundary layer. We then demonstrate the predictive application of this model with experimental data. The new model is found to account adequately for the effect of flow acceleration on the IBL development in the outer region.

Funding. Support from NERC under the agreement ASSURE: Across-Scale processes in Urban Environments (NE/W002825/1) is gratefully acknowledged.

Declaration of interests. The authors report no conflict of interest.

Data availability statement. No new data were created in this publication. The data analysed are available from https://doi.org/10.17605/OSF.IO/GCJ6V and https://doi.org/10.17605/OSF.IO/KH58X

References

Alfredsson, P.H., Segalini, A. & Örlü, R. 2011 A new scaling for the streamwise turbulence intensity in wall-bounded turbulent flows and what it tells us about the 'outer' peak. *Phys. Fluids* **23** (4), 041702.

Antonia, R.A. & Luxton, R.E. 1971 The response of a turbulent boundary layer to a step change in surface roughness Part 1. Smooth to rough. *J. Fluid Mech.* **48** (4), 721–761.

BAKLANOV, A.A., GRISOGONO, B., BORNSTEIN, R., MAHRT, L., ZILITINKEVICH, S.S., TAYLOR, P., LARSEN, S.E., ROTACH, M.W. & FERNANDO, H.J.S. 2011 The nature, theory, and modeling of atmospheric planetary boundary layers. *Bull. Am. Meteorol. Soc.* **92** (2), 123–128.

BOU-ZEID, E., ANDERSON, W., KATUL, G.G. & MAHRT, L. 2020 The persistent challenge of surface heterogeneity in boundary-layer meteorology: a review. *Boundary-Layer Meteorol.* **177** (2–3), 227–245.

BRÜMMER, B. & THIEMANN, S. 2002 The atmospheric boundary layer in an Arctic winter time on-ice air flow. *Boundary-Layer Meteorol.* **104** (1), 53–72.

CASTRO, I.P., SEGALINI, A. & ALFREDSSON, P.H. 2013 Outer-layer turbulence intensities in smooth-and rough-wall boundary layers. *J. Fluid Mech.* **727**, 119–131.

DING, S.-S., CARPENTIERI, M., ROBINS, A. & PLACIDI, M. 2024 Statistical properties of neutrally and stably stratified boundary layers in response to an abrupt change in surface roughness. *J. Fluid Mech.* **986**, A4.

DING, S.-S., PLACIDI, M., CARPENTIERI, M. & ROBINS, A. 2023 Neutrally-and stably-stratified boundary layers adjustments to a step change in surface roughness. *Exp. Fluids* **64** (4), 86.

ELLIOTT, W.P. 1958 The growth of the atmospheric internal boundary layer. *EOS Trans. AGU* **39** (6), 1048–1054.

FLACK, K.A., SCHULTZ, M.P. & SHAPIRO, T.A. 2005 Experimental support for Townsend's Reynolds number similarity hypothesis on rough walls. *Phys. Fluids* **17** (3), 035102.

FLACK, K.A., SCHULTZ, M.P. & CONNELLY, J.S. 2007 Examination of a critical roughness height for outer layer similarity. *Phys. Fluids* **19** (9), 095104.

GARRATT, J.R. 1990 The internal boundary layer – a review. *Boundary-Layer Meteorol.* **50** (1–4), 171–203.

GUL, M. & GANAPATHISUBRAMANI, B. 2022 Experimental observations on turbulent boundary layers subjected to a step change in surface roughness. *J. Fluid Mech.* **947**, A6.

HANCOCK, P.E. & HAYDEN, P. 2018 Wind-tunnel simulation of weakly and moderately stable atmospheric boundary layers. *Boundary-Layer Meteorol.* **168** (1), 29–57.

JONES, M.B., MARUSIC, I. & PERRY, A.E. 2001 Evolution and structure of sink-flow turbulent boundary layers. *J. Fluid Mech.* **428**, 1–27.

LI, M., DE SILVA, C.M., CHUNG, D., PULLIN, D.I., MARUSIC, I. & HUTCHINS, N. 2022 Modelling the downstream development of a turbulent boundary layer following a step change of roughness. *J. Fluid Mech.* **949**, A7.

MARUSIC, I., CHAUHAN, K.A., KULANDAIVELU, V. & HUTCHINS, N. 2015 Evolution of zero-pressure-gradient boundary layers from different tripping conditions. *J. Fluid Mech.* **783**, 379–411.

MIYAKE, M. 1965 Transformation of the atmospheric boundary layer over inhomogeneous surfaces. *Sci. Rep.* 5R-6, Univ. of Washington, Seattle, USA.

MONIN, A.S. & OBUKHOV, A.M. 1954 Osnovnye zakonomernosti turbulentnogo peremeshivanija v prizemnom sloe atmosfery (Basic laws of turbulent mixing in the atmosphere near the ground). *Trudy geofiz. inst. AN SSSR* **24** (151), 163–187.

SAVELYEV, S. & TAYLOR, P.A. 2001 Notes on an internal boundary-layer height formula. *Boundary-Layer Meteorol.* **101** (2), 293–301.

SAVELYEV, S. & TAYLOR, P.A. 2005 Internal boundary layers: I. Height formulae for neutral and diabatic flows. *Boundary-Layer Meteorol.* **115** (1), 1–25.

SCHULTZ, M.P. & FLACK, K.A. 2001 Outer layer similarity in fully rough turbulent boundary layers. *Exp. Fluids* **38** (3), 328–340.

TOWNSEND, A.A.R. 1976 *The Structure of Turbulent Shear Flow*. Cambridge University Press.

WILLIAMS, O., HOHMAN, T., VAN BUREN, T., BOU-ZEID, E. & SMITS, A.J. 2017 The effect of stable thermal stratification on turbulent boundary layer statistics. *J. Fluid Mech.* **812**, 1039–1075.